

The impact of environmental noise on animal communication: pattern formation in a class of deterministic and stochastic hyperbolic models for self-organised biological aggregations

Raluca Eftimie

Department of Mathematics, University of Dundee

Dundee, DD1 4HN, UK

reftimie@maths.dundee.ac.uk

Received: 19 April 2018, accepted: 21 July 2018, published: 10 August 2018

Abstract—The collective movement of animals occurs as a result of communication between the members of the community. However, inter-individual communication can be affected by the stochasticity of the environment, leading to changes in the perception of neighbours and subsequent changes in individual behaviour, which then influence the overall behaviour of the animal aggregations. To investigate the effect of noise on the overall behaviour of animal aggregations, we consider a class of nonlocal hyperbolic models for the collective movement of animals. We show numerically that for some sets of model parameters associated with individual communication, strong noise does not influence the spatio-temporal pattern (i.e., travelling aggregations) observed when all neighbours are perceived with the same intensity (i.e., the environment is homogeneous). However, when neighbours ahead/behind are perceived differently by a reference individual, noise can lead to the destruction of the spatio-temporal pattern. Moreover, we show that the increase in noise that affects individual turning

behaviours can lead to different transitions between different spatio-temporal patterns, and these transitions are relatively similar to the transitions between patterns observed when we perturb deterministically the parameters controlling individual turning.

Keywords—stochastic and deterministic nonlocal hyperbolic models, self-organised biological aggregations, animal communication

I. INTRODUCTION

Anthropogenic (i.e., human-generated) noise is known to have an impact on both individual animals as well as whole populations [1]. For example, noise affects individuals by impacting various processes related to developmental, immunological and physiological functioning [2], by decreasing the accuracy of inter-individual communication [1], [3], or by increasing their energetic costs (as animals try to move away from noise and change feeding patterns) [4]. At population level, animals

Copyright: © 2018 Eftimie. This article is distributed under the terms of the Creative Commons Attribution License (CC BY 4.0), which permits unrestricted use, distribution, and reproduction in any medium, provided the original author and source are credited.

Citation: Raluca Eftimie, The impact of environmental noise on animal communication: pattern formation in a class of deterministic and stochastic hyperbolic models for self-organised biological aggregations, *Biomath* 7 (2018), 1807217, <http://dx.doi.org/10.11145/j.biomath.2018.07.217>

might change their habitat use or their migration and behavioral patterns, or they can even lose the coordination of their social activities [1]. All these aspects are coordinated at population level via inter-individual communication. Since noise reduces the probability that neighbours detect communication signals, many animals have devised ways of increasing signal detection. For example, the free-living territorial *Anolis* lizards might add an “alert” component at the beginning of their visual communication to attract the attention of receivers, which is then followed by the detailed message component [3]. California ground squirrels can modify their communication by shifting acoustic energy in their calls to harmonics that do not overlap with highway noise [1]. Other animals, such as killer whales, increase their call amplitude in response to vessel noise [5].

While the effect of noise on individual-level behaviours is easier to study experimentally (e.g., by investigating separately the different phases of communication, namely signal production, transmission and reception, as well as by investigating the changes in individual behaviour following changes in the environment [6]), its effect on collective behaviours is more difficult to investigate due to the continuous social interactions between the members of the community (which involves continuous changes in individual behaviour in response to neighbours’ behaviours). Mathematical and computational models for the collective movement of animals can be used to generate and test hypotheses regarding the effect of environmental noise on animal behaviours. In fact, the effect of noise has been considered by the majority of individual-based models (i.e., models that track the position and velocity/orientation of individual members of a group) in the literature of collective movement; see, for example, [7], [8], [9], [10], [11], [12], [13], [14] and the references therein. All these individual-based studies assume that noise impacts the velocity or the movement direction of individuals. However, given that there are not too many analytical techniques to investigate these individual-based models, a few

other studies started focusing on partial differential equation (PDE) models (i.e., models that describe the changes in the density of individuals over space and time) for self-organised collective movement in animals or humans that incorporate environmental noise. In many situations, the PDEs were obtained from the individual-based models, in the limit for large particle numbers, in which case the stochastic terms were approximated by diffusion processes (see [15] for a review of such modelling approaches). One of the few PDEs (of parabolic type) for collective movement in biology that included explicitly a stochastic term was introduced in [16]. Nevertheless, we need to emphasise that in the mathematical literature there are a few studies on stochastic PDE models (for various problems in physics or biology – but not necessarily collective movement), which focus mostly on existence, uniqueness and stability questions; see for example the studies on stochastic parabolic models [17] or the studies on stochastic first-order local conservation laws [18], [19], [20]. It is worth mentioning that the majority of these studies focus almost exclusively on local models.

Here we consider a class of nonlocal first-order hyperbolic models previously introduced in [21], [22], [23] to investigate pattern formation in self-organised animal aggregations in response to inter-individual communication. We need to emphasise that first-order local and nonlocal hyperbolic systems (also called discrete velocity/orientation Boltzmann models, since they are similar to the kinetic Boltzmann equation when orientation is reduced to only two directions, right (+) and left (–) [24]), have been developed for almost three decades to describe collective movement in ecology and cell biology; see for example [25], [26], [27], [28], [29], [30] and references therein. The majority of these hyperbolic models are deterministic, thus being easier to investigate analytically in terms of existence and uniqueness of solutions [27], [28], [23], or bifurcation of patterns [23]. For a review of mathematical aspects of discrete-velocity Boltzmann-like equations, see [31]. In our current study, since anthropogenic noise can

disrupt animal communication and thus affect collective movement, we generalise the deterministic hyperbolic models in [21], [22] by assuming that white noise is incorporated (multiplicatively) into the terms that account for the perception of surrounding neighbours, as well as in the terms that describe turning behaviours during movement (as for the individual-based models mentioned above). To our knowledge, there are no studies that focus on the effect of multiplicative noise in nonlocal hyperbolic models for collective movement, and therefore this modelling approach together with preliminary simulation results presented in this study open new doors regarding possible directions of analytical investigation of the various dynamics exhibited by these nonlocal stochastic models.

This paper is structured as follows. In Section II we describe the class of nonlocal 1D models introduced in [21], [22] and discuss separately the newly added noise terms. Then, in Section III we discuss the number and stability of spatially-heterogeneous steady states exhibited by the deterministic version of the models (to identify the effects of deterministic perturbations of individual turning behaviour, and deterministic perturbations of neighbours perception, on the instability of steady states). In Section IV we show numerical results for different types of spatio-temporal patterns that can be affected by noise with different strength levels, and identify transitions between different types of patterns, or between spatial pattern and spatially homogeneous states. We conclude in Section V with a summary and discussion of results.

II. MODEL DERIVATION

Following the approach in [21], [22], [32], we consider a 1D finite domain $[0, L]$ on which we assume that we have an animal population formed of left-moving ($u^-(x, t)$) and right-moving ($u^+(x, t)$) densities of animals. (This setting could describe, for example, a population of fish moving through human-made corridors such as shipping canals [33], [34].) The dynamics of this population is described by the following nonlocal conservation

laws:

$$\frac{\partial u^+}{\partial t} + \gamma \frac{\partial u^+}{\partial x} = -\lambda^+[u^+, u^-]u^+ + \lambda^-[u^+, u^-]u^-, \tag{1a}$$

$$\frac{\partial u^-}{\partial t} - \gamma \frac{\partial u^-}{\partial x} = \lambda^+[u^+, u^-]u^+ - \lambda^-[u^+, u^-]u^-. \tag{1b}$$

Here we assume that individuals in both populations move with constant velocities γ (i.e., u^+ move right with velocity $+\gamma$, while u^- move left with velocity $-\gamma$), and can change movement direction either randomly or in a directed manner following interactions (via communication) with their neighbours; see Figure 1(a). (Note that the importance of adapting velocity and turning behaviour during fish movement has been emphasised in various experimental studies [35], [36].) The density-dependent turning functions λ^\pm (which connect the left-moving population u^- to the right-moving population u^+) are given as follows:

$$\lambda^\pm[u^+, u^-] = \lambda_1 + \lambda_2 f^\pm[u^+, u^-], \tag{2}$$

with λ_1 and λ_2 constants that are approximating the random and directed changes in individuals movement direction (see also [21]). The functionals f^\pm describe the nonlocal interactions between individuals placed at different positions in space (i.e., within repulsive, attractive and alignment ranges; see Figure 1(b)) – as these interactions determine whether an individual turns around or not, towards/away from its neighbours. We assume that f^\pm are non-negative and increasing functions of the nonlocal interactions among individuals [21], [22], which are also almost zero when there are no any neighbours nearby (i.e., $f^\pm[0, 0] \approx 0$). One function that satisfies all these conditions is

$$f^\pm[u^+, u^-] = 0.5 + 0.5 \tanh \left(y_r^\pm[u^+, u^-] + y_{al}^\pm[u^+, u^-] + y_a^\pm[u^+, u^-] - y_0 \right), \tag{3}$$

where constant y_0 was chosen such that $f^\pm[0, 0] \approx 0$ [21], [22]. The nonlocal social interaction terms $y_{r,al,a}^\pm$ (for the right-moving (+) and left-moving (-) individuals) are described in detail in Table I. In this study we focus only on the case of

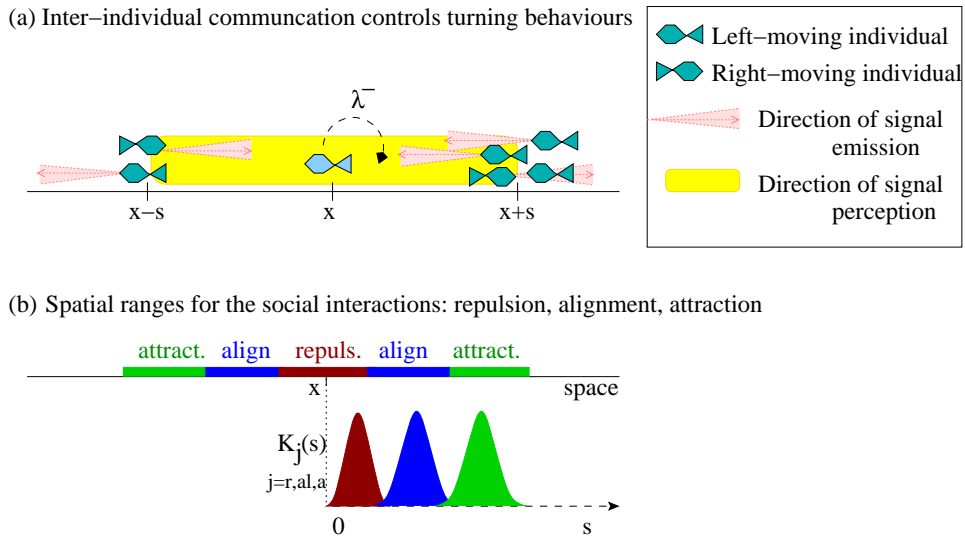


Fig. 1. (a) Description of inter-individual communication (shown is omni-directional signal perception by a reference individual at x , and uni-directional signal emission by neighbours at $x \pm s$) For other types of inter-individual communication see [22], [32]; (b) Spatial ranges for three different social interactions: repulsion (r), alignment (al), attraction (a). These interaction ranges are described by spatial kernels $K_j(s)$, $j = r, a, al$ (see equations (4)).

omni-directional signal perception (by a reference individual at x) and uni-directional signal emission (by its neighbours at $x \pm s$); see also Figure 1(a). This leads to the following assumptions regarding these interactions:

- Due to the omni-directionality in signal perception, the attraction/repulsion interactions depend on the total number of neighbours ($u = u^+ + u^-$) positioned left ($x - s$) and right ($x + s$) of a reference individual at x . To describe the turning behaviour of a right-moving reference individual ($u^+(x, t)$), we note that if $u(x + s) > u(x - s)$ (i.e., more neighbours ahead relative to the moving direction), if these neighbours are within the repulsion range ($K_r(s)$) then the reference individual will turn around to avoid collision (i.e., $y_r^+ > 0$, which increases the value of f^+ and λ^+). In contrast, if these neighbours are within the attraction range ($K_a(s)$) then the reference individual will keep moving in the same direction to join its neighbours at $x + s$ (i.e., $y_r^+ < 0$, which decreases the value of f^+ and λ^+ , and thus reduces the probability

of turning). Moreover, since attraction and repulsion have opposite effects, they enter the integral terms in Table I with opposite signs. Note also that in Table I, the densities of neighbours at $x \pm s$ are multiplied with the perception intensities of these neighbours ($p_{a,b}$), to account for the possible heterogeneity of the environment. We will describe $p_{a,b}$ in more detail shortly.

- Again, due to the omni-directionality in signal perception, the alignment interactions depend on all left-moving ($u^-(x \pm s)$) and right-moving ($u^+(x \pm s)$) neighbours. A reference right-moving individual $u^+(x, t)$ will decide whether to turn around, depending on the density of left-moving/right-moving neighbours ahead at $x + s$ (i.e., $u^-(x + s) - u^+(x + s)$) and behind at $x - s$ (i.e., $u^-(x - s) - u^+(x - s)$). If there are more right-moving neighbours than left-moving neighbours, then the reference individual $u^+(x, t)$ will keep moving in the same direction (since $y_{al}^+ < 0$, which decreases f^+ and λ^+). Otherwise, if there are more left-moving neighbours, the reference individual $u^+(x, t)$ will turn around to follow

TABLE I

NONLOCAL TERMS FOR THE THREE SOCIAL INTERACTIONS THAT AFFECT THE RIGHT-MOVING (+) AND LEFT-MOVING (-) INDIVIDUALS: REPULSION (y_r^\pm), ALIGNMENT (y_{al}^\pm), ATTRACTION (y_a^\pm). WE ASSUME THAT A REFERENCE INDIVIDUAL CAN PERCEIVE (THROUGH THE INTEGRATION OF MULTIPLE STIMULI: E.G., VISUAL, AUDITORY) ALL ITS NEIGHBOURS AHEAD AND BEHIND IT; SEE ALSO FIGURE 1(A). WE DENOTE THE TOTAL DENSITY OF INDIVIDUALS AT POSITION x AND TIME t BY: $u(x, t) = u^+(x, t) + u^-(x, t)$.

repulsion	$y_r^\pm[u^+, u^-] = \pm q_r \int_0^\infty K_r(s)(p_a u(x \pm s) - p_b u(x \mp s)) ds$
attraction	$y_a^\pm[u^+, u^-] = \mp q_a \int_0^\infty K_a(s)(p_a u(x \pm s) - p_b u(x \mp s)) ds$
alignment	$y_{al}^\pm[u^+, u^-] = \pm q_{al} \int_0^\infty K_{al}(s) \left(p_a (u^\mp(x \pm s) - u^\pm(x \pm s)) + p_b (u^\mp(x \mp s) - u^\pm(x \mp s)) \right) ds$

these neighbours. Here, we use the word “individual” in a very loose sense, since $u^+(x, t)$ actually describe the density of individuals.

For other types of possible communication mechanisms that can be incorporated into equations (1)-(3) we direct the reader to [22], [32].

The coefficients q_j , $j = r, al, a$ that appear in $y_{r,al,a}^\pm$ (in front of the integrals in Table I), describe the strengths of the three social interactions, while K_j are the kernels that describe the spatial ranges for these three social interactions (see also Figure 1(b) and Table II). Throughout this study we will consider the following interaction kernels [21]:

$$K_j(s) = \frac{1}{2\pi m_j^2} e^{-(s-s_j)^2/(2m_j^2)}, \quad (4)$$

$j = r, al, a$, and $m_j = s_j/8$.

The meaning and values of parameters m_j and s_j that define the interaction ranges are given in Table II.

Finally, the parameters p_a and p_b that appear inside the integrals in Table I are describing the perception strength of neighbours positioned at $x \pm s$. In a homogeneous environment, all neighbours positioned left/right with respect to a reference individual at x are perceived the same way (in the case of omni-directional perception), and thus $p_a = p_b$; see also Figure 2(a). However,

in a heterogeneous environment, the neighbours positioned left/right of the reference individual are perceived differently, depending on the spatial heterogeneity (e.g., wind blowing from one direction, ensuring clear auditory signals from that particular direction), and thus $p_a \neq p_b$; see also Figure 2(b).

To complete the derivation of model (1)-(4), we need to specify the boundary conditions on the finite domain $[0, L]$. Taking the same approach as in [21], [22], we will assume periodic boundary conditions (corresponding to an arena-type domain):

$$u^+(L, t) = u^+(0, t), \quad u^-(0, t) = u^-(L, t). \quad (5)$$

The Effect of Noise: To investigate the effect of anthropogenic noise on the dynamics of model (1)-(3), we assume that in the presence of noise the individuals try to increase the detection of signals emitted by their neighbours (and thus try to increase neighbours’ perception $p_{a,b}$). Moreover, in the presence of noise, individuals try to increase their changes in movement directions (to ensure that they can detect better neighbours from all directions). Thus, we will consider the following cases:

- 1) Noisy environment affects the perception of neighbours: $p_{a,b} = p_{a,b}^* + W(t)$, where the noise $W(t)$ is a random value chosen (at

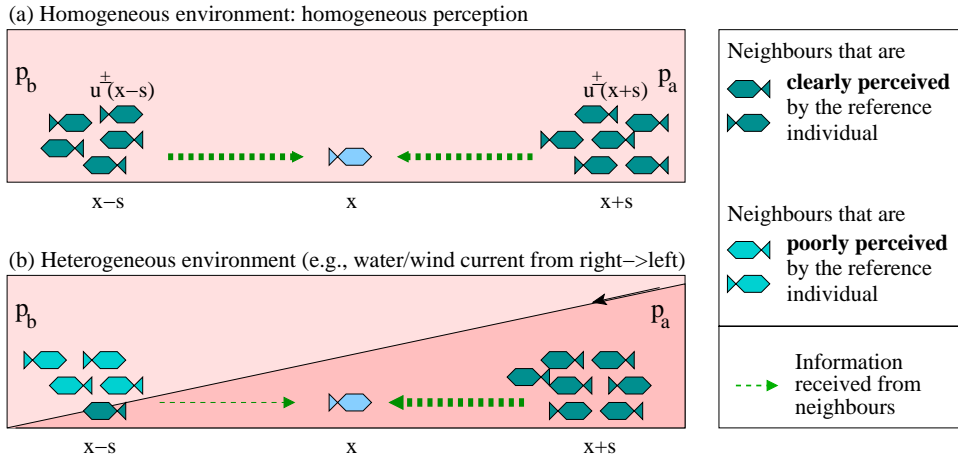


Fig. 2. Caricature description of (a) a homogeneous environment, where all neighbours are perceived with the same intensity: $p_a = p_b$; and (b) a heterogeneous environment, where some neighbours are perceived better than others: $p_a > p_b$ (e.g., wind blowing from the right, carrying sound further away in a clear manner).

- every time step t) with a uniform probability within the interval $[0, n_m]$ (where $n_m \leq 1$);
- 2) Noisy environment affects the turning rates (i.e., direction of movement): $\lambda_{1,2} = \lambda_{1,2}^* + W(t)$, where the noise $W(t)$ is a random value chosen with a uniform probability within the interval $[0, n_m]$;
 - 3) Finally, we will also discuss briefly the assumption that the noise can increase as well as decrease the perception of neighbours: $p_{a,b} = p_{a,b}^* + W_1(t)$, where the noise $W_1(t)$ is a random value chosen with a uniform probability within the interval $[-n_m, n_m]$, with $n_m \leq 1$. Note that this noise term is similar to the one introduced by Vicsek et al. in [8], for individual-based models.

Remark 1. *Since we focus on a time scale that ignores any birth/death processes, model (1) conserves the total population density [32]. Let us denote this total population density by $A = (1/L) \int_0^L (u^+(x, t) + u^-(x, t)) dx$.*

Remark 2. *In [32] we showed how can we derive the nonlocal model (1) using a correlated random walk approach (i.e., a stochastic process different from the classical Brownian motion during which the directions of motion for successive time steps are uncorrelated [37]). In a probabilistic setting,*

this correlated random walk approach leads to solutions that can be seen as probability densities ($u^\pm(x, t) := u(x, \pm, t) \geq 0$, $\int_{-\infty}^{\infty} u^\pm(x, t) dx = 1$ [37]). Moreover, in this context, parameters $\lambda_{1,2}$ correspond to the probabilities of turning randomly or in a directed manner. The incorporation of noise terms $W(t)$ and $W_1(t)$ into model (1) – via parameters $p_{a,b}$ or $\lambda_{1,2}$ – adds another layer of complexity, generating a sort of double stochasticity.

III. DETERMINISTIC MODEL:

SPATIALLY-HOMOGENEOUS STATES AND THEIR LINEAR STABILITY

We start the investigation of model (1) by focusing on the deterministic model (i.e., $W(t) = 0$, $W_1(t) = 0$), and investigating the number and stability of spatially homogeneous steady states (i.e., states characterised by individuals spread over the whole domain). We will use this information in the next section, to better understand the formation of spatio-temporal patterns in the deterministic system (1).

Figure 3 shows the number of spatially homogeneous steady states (i.e., states that satisfy $\frac{\partial u^\pm}{\partial t} = \frac{\partial u^\pm}{\partial x} = 0$) exhibited by the deterministic model (1) as we vary: (a) the difference between the perception intensity of neighbours ahead and behind

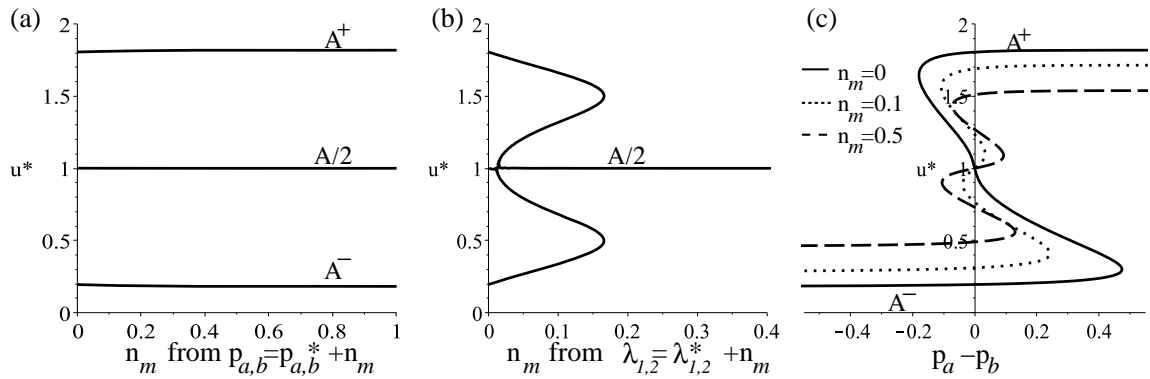


Fig. 3. Bifurcation diagram for the number of steady states exhibited by the deterministic model (1), as we vary the following parameters: (a) the value n_m in the perturbations of the perception intensities $p_{a,b} = p_{a,b}^* + n_m$; (b) the value n_m in the perturbations of the turning rates $\lambda_{1,2} = \lambda_{1,2}^* + n_m$; (c) the difference between the perception intensity of neighbours ahead and behind ($p_a - p_b$) with respect to a reference individual, when we perturb both $p_{a,b} = p_{a,b}^* + n_m$, $\lambda_{1,2} = \lambda_{1,2}^* + n_m$ with $n_m = 0.0$ (continuous curve), $n_m = 0.1$ (dotted curve) and $n_m = 0.5$ (dashed curve).

($p_a - p_b$) with respect to a reference individual; (b) the value n_m in the deterministic perturbations of the perception intensities $p_{a,b} = p_{a,b}^* + n_m$; (c) the value n_m in the deterministic perturbations of the turning rates $\lambda_{1,2} = \lambda_{1,2}^* + n_m$. (We will return to the discussion of these deterministic perturbations in the next chapter, in the context of numerical simulations.) The vertical axes in Figure 3 show $u^* = u^{*,+}$, the steady states for u^+ . Due to the symmetry of model (1), similar graphs could be obtained also for $u^{*,-} = A - u^*$ (i.e., the steady state for u^-). We denote by $u^* = A/2$ the steady state where half individuals are facing left and half are facing right, while being spread over the whole domain: $(u^{*,+}, u^{*,-}) = (A/2, A/2)$. Also, we denote by A^\pm the states where more individuals are facing one direction compared to the other direction.

We observe in Figure 3 that it is possible to obtain one, three or five steady states u^* . For example, deterministic perturbations of $\lambda_{1,2}$ change the number of steady states (panel (b)): from 3 distinct states u^* when $n_m < 0.011$, to 5 states u^* when $n_m \in (0.11, 0.16)$, and finally only one state when $n_m > 0.16$. Note that varying either $p_{a,b}$ alone or $\lambda_{1,2}$ alone preserves the symmetry of the steady state u^* with respect to $A/2$ (see panels (a),(b)), while varying the difference be-

tween $p_a - p_b$ together with $p_{a,b}$ and $\lambda_{1,2}$ breaks this symmetry (see panel (c)).

Finally, we note that the only steady state that does not depend on the model parameters is $u^* = A/2$, and this state persists as long as $p_a = p_b$. As shown in Figure 3 (c), this state vanishes for $p_a \neq p_b$.

Next, we investigate the linear stability of the spatially homogeneous steady states $(u^{*,+}, u^{*,-}) = (A/2, A/2)$, as well as the steady states $(u^{*,+}, u^{*,-}) = (A^+, A - A^+)$ or $(u^{*,+}, u^{*,-}) = (A - A^-, A^-)$. To this end, we consider small perturbations of these states: $u^\pm(x, t) = u^{*,\pm} + a_\pm e^{\sigma t + ikx}$, with $a_\pm \ll 1$. (Here σ describes the growth/decay of the perturbations, while k is the wavenumber that emerges when perturbations grow.) Substituting these expressions into the linearised system (1), leads to the following dispersion relation:

$$\sigma^2 + \sigma(c_1 + c_2 + c_3(D^- - D^+)) + (\gamma k)^2 - \gamma ik(c_1 - c_2 + c_3(D^- + D^+)) = 0, \quad (6)$$

where

$$\begin{aligned} B &= 2u^*(q_r - q_a)(p_a - p_b), \\ c_3 &= u^* \lambda_2 (f'(B) + f'(-B)), \\ c_1 &= \lambda_1 + \lambda_2 f(B), \quad c_2 = \lambda_1 + \lambda_2 f(-B), \end{aligned}$$

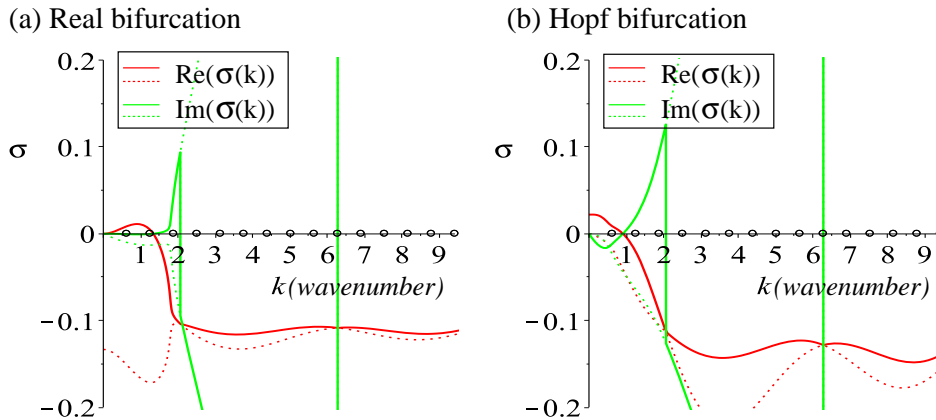


Fig. 4. Real and imaginary parts of $\sigma(k)$, for the symmetric steady state $(A/2, A/2)$, showing: (a) a real bifurcation (for $q_a = 0.6$, $\lambda_2 = 0.9$ and all other parameters as in Table II); (b) a Hopf bifurcation (for $q_a = 2.0$, $\lambda_2 = 0.27$, and all other parameters as in Table II); Continuous curves show the largest eigenvalue ($\sigma_1(k)$), while the dotted curves show the smallest eigenvalue ($\sigma_2(k)$). The circles on the x-axis show the discrete wavenumbers $k_n = 2\pi n/L$, with $n = 1, 2, \dots$

$$\hat{K}^+ = \int_0^\infty (q_r K_r(s) - q_a K_a(s)) e^{iks} ds,$$

$$\hat{K}^- = \int_0^\infty (q_r K_r(s) - q_a K_a(s)) e^{-iks} ds,$$

$$\hat{K}_{al}^\pm = \int_0^\infty K_{al}(s) e^{\pm iks} ds,$$

$$D^+ = \hat{K}^+ p_a - \hat{K}^- p_b + q_{al}(\hat{K}_{al}^+ p_a + \hat{K}_{al}^- p_b),$$

$$D^- = \hat{K}^+ p_a - \hat{K}^- p_b - q_{al}(\hat{K}_{al}^+ p_a + \hat{K}_{al}^- p_b).$$

The real and imaginary components of this dispersion relation (corresponding to the steady state $(u^{*,+}, u^{*, -}) = (A/2, A/2)$) are graphed in Figure 4, for different parameter values that generate: (a) a real bifurcation (i.e., $Re(\sigma(k_1)) > 0$, $Im(\sigma(k_1)) = 0$), and (b) a Hopf bifurcation (i.e., $Re(\sigma(k_1)) > 0$, $Im(\sigma(k_1)) > 0$). The real bifurcations give rise to stationary aggregation patterns (e.g., stationary pulses), while the Hopf bifurcations give rise to moving aggregation patterns (e.g., travelling pulses). These patterns form primary solution branches, and can further bifurcate themselves forming more complex patterns, as we will discuss below.

Next, we focus on the stability of different steady states as we vary the magnitudes of the perception sensitivities $p_a^* - p_b^*$, and different deterministic perturbations (of magnitudes n_m) of baseline $p_{a,b}^*$ and $\lambda_{1,2}^*$ values (as it will be considered

later in the numerical simulations in Figures 9, 10, and 11). We see in Figure 5(a) that increasing n_m in the perception sensitivities $p_{a,b} = p_{a,b}^* + n_m$ has opposite effects on the different steady states: (i) it increases the amplitude of $Re(\sigma(k))$ for the steady state $(u^{*,+}, u^{*, -}) = (A/2, A/2)$ thus increasing the instability of this state, and (ii) it decreases the amplitude of $Re(\sigma(k))$ for the steady state $(u^{*,+}, u^{*, -}) = (A^+, A^-)$ (with $A^+ \neq A^-$) thus leading to the stability of this state. In panels (b) we see that increasing n_m in the turning rates $\lambda_{1,2} = \lambda_{1,2}^* + n_m$ has different effects compared to the previous case: (i) it decreases the amplitude of $Re(\sigma(k))$ for the steady state $(u^{*,+}, u^{*, -}) = (A/2, A/2)$ and (ii) it increases the amplitude of $Re(\sigma(k))$ for the steady state $(u^{*,+}, u^{*, -}) = (A^+, A^-)$ (with $A^+ \neq A^-$). We also note here that for large n_m the state $(A/2, A/2)$ loses the nonzero imaginary part of the eigenvalues (i.e., $Im(\sigma(k)) = 0$ for those k values where $Re(\sigma(k)) > 0$; see Figure 5(b)(i)), thus suggesting the possibility of having stationary aggregations for large n_m . Finally, we see in panels (c) that increasing the difference $p_a - p_b$ (and thus the heterogeneity of the environment) leads to lower amplitudes of $Re(\sigma(k))$, and thus to stable states. Note that for $p_a - p_b = 0.4$, all

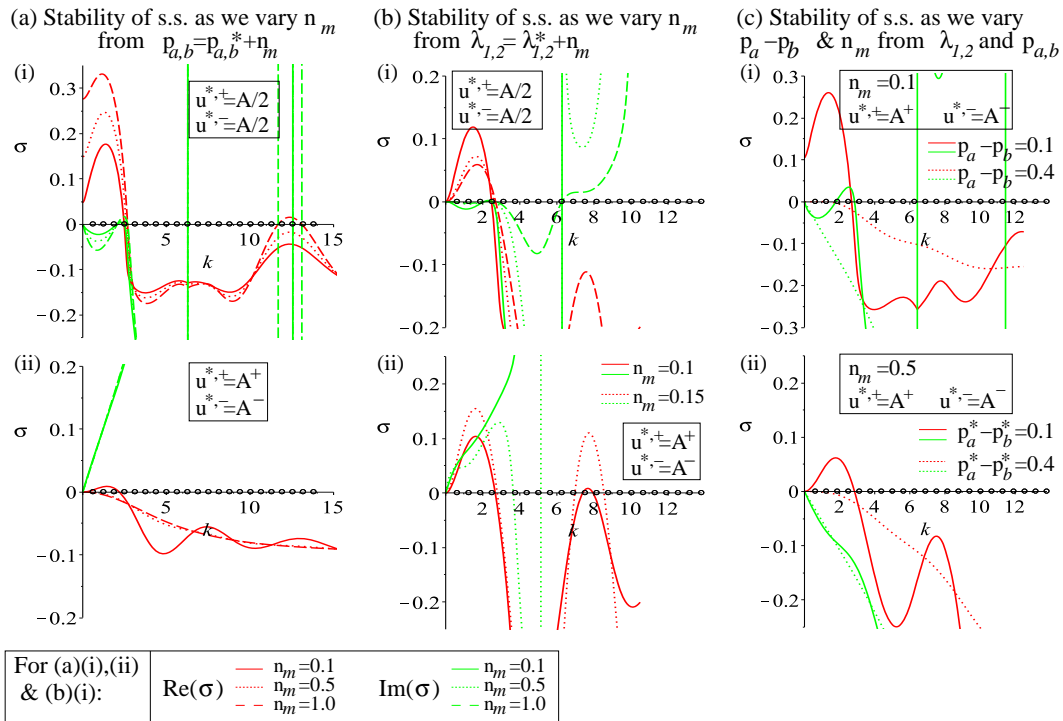


Fig. 5. Stability of various steady states (s.s.) described in Figure 3, as given by the real parts (red on coloured figures) and imaginary parts (green on coloured figures) of the largest eigenvalue in the dispersion relation $\sigma(k)$, when we vary different model parameters: (a) the magnitude of deterministic perturbation n_m from the perception terms $p_{a,b} = p_{a,b}^* + n_m$; (b) the magnitude of deterministic perturbation n_m from the turning rates $\lambda_{1,2} = \lambda_{1,2}^* + n_m$; (c) the difference between the baseline perception sensitivities of neighbours ahead (p_a^*) and behind (p_b^*), relative to the movement direction of a reference individual, as well as the magnitude of the deterministic perturbation n_m in both $\lambda_{1,2} = \lambda_{1,2}^* + n_m$, $p_{a,b} = p_{a,b}^* + n_m$.

steady states are stable (as $Re(\sigma(k)) \leq 0$).

The fact that multiple steady states can be linearly unstable at the same time complicates the analysis of the dynamics of model (1), since the nonlinear interactions (and the magnitude of the perturbations in the system) could lead to the selection and persistence of particular types of spatio-temporal patterns that can be either travelling or stationary (irrespective of the types of the bifurcation from the spatially homogeneous state: real or Hopf bifurcations). These persistent spatio-temporal patterns arise from secondary bifurcations from the primary solution branches.

As we show next, these stability results (obtained via the dispersion relation (6)) support the numerical simulation results in Figures 9, 10, and 11 (for both the deterministic version of model (1), and its stochastic version with $W(t) \neq 0$).

IV. NUMERICAL RESULTS

In the following we describe some of the spatio-temporal patterns that can be exhibited by the deterministic and stochastic model (1)-(3) (i.e., with $W(t) = 0$ and $W(t) \neq 0$). For the numerical simulations, we discretised the domain using a space step $\Delta x = 0.01$ and a time step $\Delta t = 0.02$ (which ensures that the Courant-Friedrichs-Lewy condition holds). The integrals were approximated using Simpson's method [38] (and were wrapped around the domain to implement the periodic boundary conditions), while the advection part in the left-hand-side of equations (1), was discretised using a classical predictor-corrector MacCormack method. The noise $W(t)$ (in the $p_{a,b}$ and $\lambda_{1,2}$ terms; see cases (I) and (II) in model description) was implemented by choosing at every time step

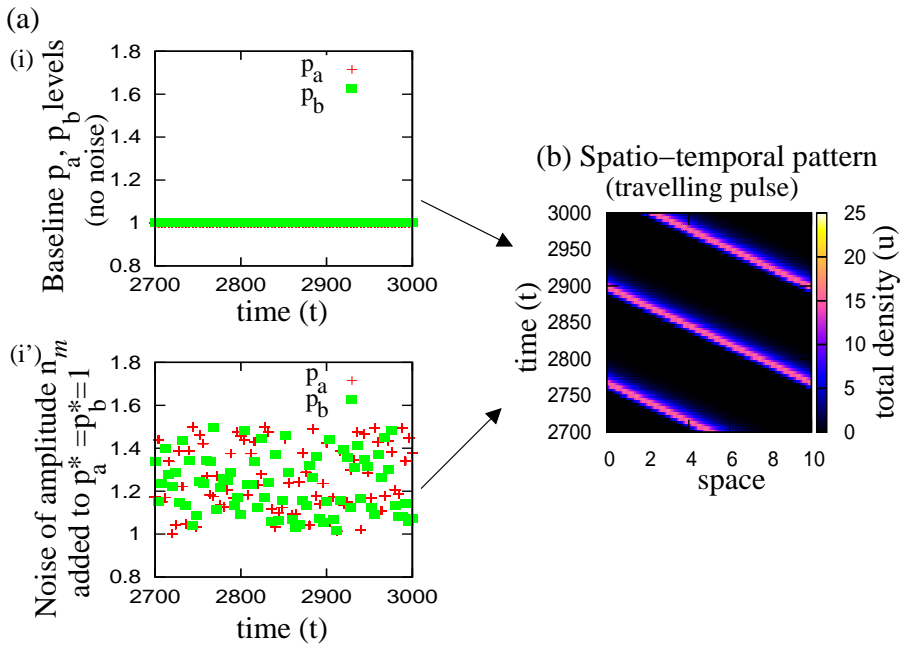


Fig. 6. (a) Perception levels p_a and p_b when: (i) no noise (i.e., $p_{a,b} = p_{a,b}^*$, $W(t) = 0$, $W_1(t) = 0$), and (i') noise levels $W(t) = \text{Rand}(0, 0.5)$ of maximum amplitude $n_m = 0.5$ added to the baseline $p_{a,b}^* = 1$ values: $p_{a,b}^* + \text{Rand}(0, 0.5)$. (ii) Spatio-temporal pattern for the total density $u = u^+ + u^-$, which occurs for both baseline $p_{a,b}$ values (as in (i)), and randomly-perturbed $p_{a,b}$ values (as in (i')). This travelling pulse pattern describes persistent moving aggregations.

Δt a random number uniformly distributed in the interval $[0, n_m]$, with $n_m \leq 1$ (i.e., $W(t) = \text{Rand}(0, n_m)$). Finally, the noise $W_1(t)$ (in the $p_{a,b}$ terms; see case (III) in model description) was implemented by choosing at every time step Δt a random number uniformly distributed over the interval $[-n_m, n_m]$, with $n_m \leq 1$ (i.e., $W_1(t) = \text{Rand}(-n_m, n_m)$). The initial conditions for the numerical simulations shown below are random perturbations of the spatially-homogeneous steady state $(u^{*,+}, u^{*,-}) = (A/2, A/2)$ (where $A = 2$ throughout this study). Finally, the values of the parameters used throughout these numerical simulations are summarised in Table II.

A. The effect of noise on the perception of neighbours

a) *Homogeneous environment:* We start the numerical investigation of model (1) by considering first a homogeneous environment (i.e., $p_a^* = p_b^* = 1$; see also Figure 2(a)). In this case (and for the parameter values described in Table II) the

simulations in Figure 6(ii) show the persistence of travelling aggregations irrespective of the noise level (and irrespective of the presence/absence of the noise added to p_a^* and p_b^* parameters).

b) *Heterogeneous environment:* Next, we investigate the effect of a heterogeneous environment (i.e., $p_a \neq p_b$; see also Figure 2(b)). Figure 7 shows that for a heterogeneous environment, the increase in the noise level (from (a) $W(t) = \text{Rand}(0, 0.1)$ to (b) $W(t) = \text{Rand}(0, 0.5)$), which here leads to an increase in the perception of neighbours, destroys the formation and persistence of moving aggregations. However, assuming that noise can also decrease the perception of neighbours (i.e., $W_1(t) = \text{Rand}(-0.5, 0.5)$), preserves the original pattern. Therefore, it is possible that the heterogeneity of the environment (which leads to poorer perception of some neighbours) combined (non-linearly) with the noise which could increase as well as decrease the perception of some neighbours, might preserve the travelling

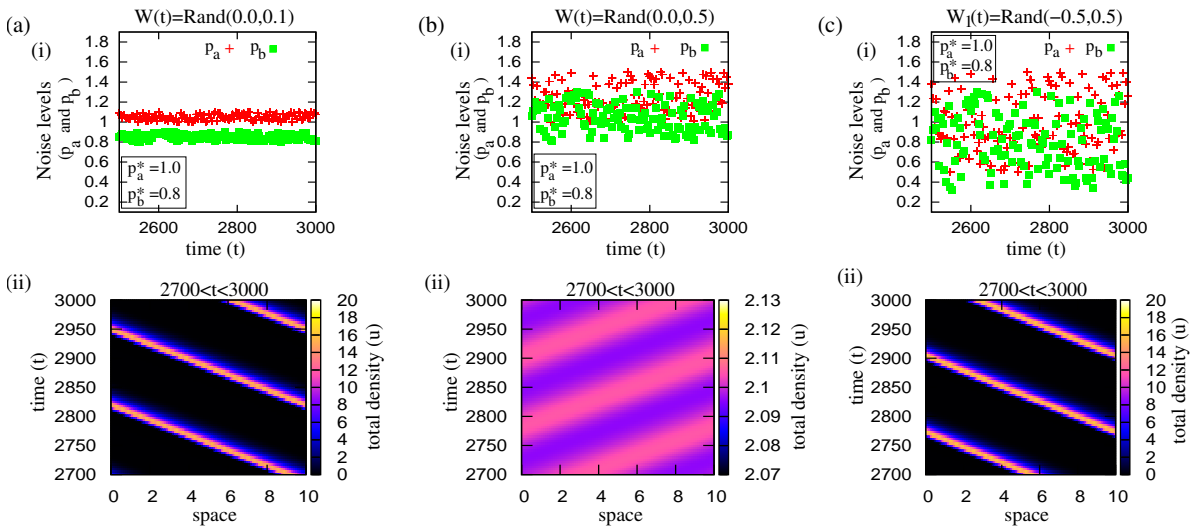


Fig. 7. Pattern formation in a heterogeneous environment ($p_a^* = 1.0$, $p_b^* = 0.8$), as we increase the noise level in p_a and p_b . (a) $W(t) = \text{Rand}(0, 0.1)$: $p_a = 1.0 + W(t)$, $p_b = 0.8 + W(t)$; (b) $W(t) = \text{Rand}(0, 0.5)$: $p_a = 1.0 + W(t)$, $p_b = 0.8 + W(t)$; (c) $W_1(t) = \text{Rand}(-0.5, 0.5)$: $p_a = 1.0 + W_1(t)$, $p_b = 0.8 + W_1(t)$.

aggregation pattern.

To have a better understanding on the decreasing/increasing effects of noise on the perception of neighbours, and on the preservation of patterns, in Figure 8 we summarise the patterns obtained in homogeneous vs. heterogeneous environments, for various p_a^* and p_b^* baseline values with noise of maximum amplitudes $n_m = 0.5$: (a) $W(t) = \text{Rand}(0, 0.5)$, and (b) $W_1(t) = \text{Rand}(-0.5, 0.5)$. We observe that, by assuming that noise can both decrease and increase the perception of neighbours (panel (b)), it is possible to have persistence of patterns in strong heterogeneous environments (e.g., large $p_a^* > p_b^*$ or $p_b^* > p_a^*$). We also observe that because of the symmetry of the model, it does not matter the direction of the environmental heterogeneity (i.e., $p_a^* > p_b^*$ or $p_b^* > p_a^*$).

B. The effect of noise on the turning rates

Next, we assume that the environmental noise can affect the turning rates λ_1 and λ_2 . Figure 9(a)-(c) shows the types of spatio-temporal patterns exhibited by model (1) as we vary the amplitude of the noise: $W(t) = \text{Rand}(0, n_m)$, with $n_m \in [0.1, 1]$. We note three different types of patterns: (a) stationary pulses (with very high

amplitudes; for $n_m > 0.725$); (b) chaotic zigzags (with amplitudes varying over wide ranges; for $n_m \in (0.725, 0.2)$); (c) travelling pulses (with low amplitudes; for $n_m < 0.2$). In panel (d) we show the maximum local amplitudes (calculated at every time step $t \in 1700 - 2000$) of the spatio-temporal patterns obtained as we decrease the noise amplitude n_m from 1 to 0.1. The zigzags are characterised by amplitudes that vary between a wide range (20 and 40-45), due to the changes in moving directions that take place over a few time steps, and which impact the spatial distributions of individuals inside the moving aggregations. In contrast, the travelling and stationary pulses are characterised by amplitudes that span much narrower ranges, suggesting that during these two types of behaviours the aggregations are more compact, and there is no significant change in the spatial distribution of individuals inside the aggregations (again, the small variations in the amplitude of the patterns are the result of the individual turning behaviour $\lambda_{1,2} > 0$).

In Figure 9(d) we observe that for low noise (i.e., $n_m \in (0.1, 0.2)$) there are actually two branches for travel pulse dynamics: the upper (red

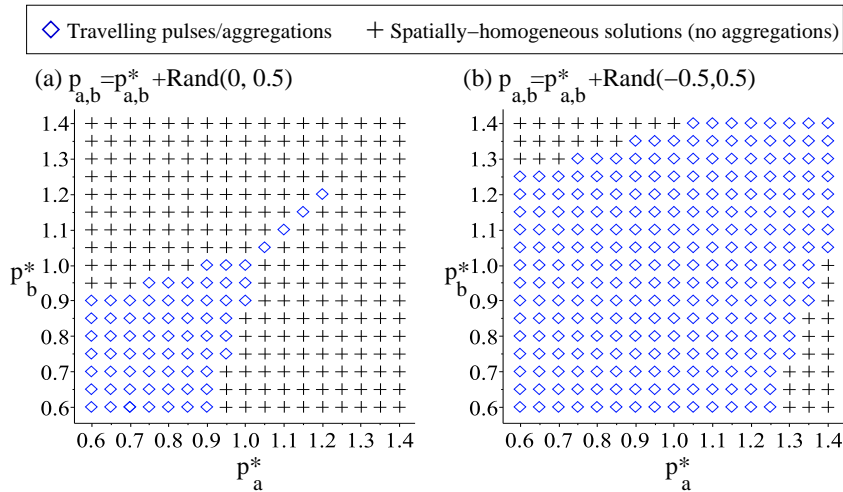


Fig. 8. Summary of patterns exhibited by model (1) in the parameter space determined by the baseline values for $p_{a,b} \in [0.6, 1.5]$, where the perception terms are (a) $p_{a,b} = p_{a,b}^* + W(t)$, with $W(t) = \text{Rand}(0, 0.5)$; (b) $p_{a,b} = p_{a,b}^* + W_1(t)$, with $W_1(t) = \text{Rand}(-0.5, 0.5)$.

branch was obtained starting with $n_m = 1.0$ and decreasing it to $n_m = 0.1$, while the lower branch was obtained starting with $n_m = 0.1$ and increasing it up to $n_m = 1.0$. These two branches characterise a hysteresis-like behaviour: starting with high noise ($n_m = 1$) and decreasing it below $n_m = 0.2$ leads to high-amplitudes ($\in (20, 24)$) travelling pulse patterns; on the other hand starting with $n_m = 0.1$ and increasing it leads to lower-amplitudes ($\in (10, 12)$) travelling pulse patterns. This bifurcation result suggests that these branches of travelling pulses co-exist at the same time, and which one is attained depends on the initial conditions.

Since the patterns in Figure 9 were obtained when we perturbed $\lambda_{1,2}^*$ with a non-negative (normally distributed) random variable $W(t)$ of maximum amplitude n_m , to check whether the transitions between patterns are indeed the result of noise, next we investigate what happens when we perturb $\lambda_{1,2}^*$ with a deterministic value $n_m \in [0.1, 1]$ (i.e., $W(t) = 0$, and $\lambda_{1,2} = \lambda_{1,2}^* + n_m$).

Figures 10(a)-(c) show that similar types of spatio-temporal patterns can emerge for deterministic $\lambda_{1,2}$ values. However, the numerically-computed bifurcation structure of the deterministic system is slightly different compared to the bi-

furcation structure of the stochastic system (see panel (d)). More precisely, the deterministic system seems to exhibit multiple stable branches of spatially-heterogeneous stationary solutions for $n_m \in (0.525, 1)$, and one can reach these solution branches starting with different n_m parameters. For example, starting with $n_m = 0.1$ and increasing it towards $n_m = 1$ leads to an upper branch of high-amplitude stationary pulses, while starting with $n_m = 1$ and decreasing it towards $n_m = 0.1$ leads to a lower branch of low-amplitude stationary pulses (as in panel (a)). Moreover, the parameter range where the zigzags occur is slightly different for the deterministic system ($n_m \in (0.175, 0.525)$) compared to the stochastic system ($n_m \in (0.2, 0.75)$).

Remark 3. *These numerical results on pattern formation (for the deterministic system) are supported by the linear stability results discussed in Figure 5(b): for the steady state $(u^{*,+}, u^{*, -})$, low n_m can give rise (via Hopf bifurcations) to travelling patterns, while high n_m can give rise (via real bifurcations) to stationary patterns. We emphasise that these travelling and stationary patterns that arise from Hopf or real bifurcations form primary bifurcation branches. However,*

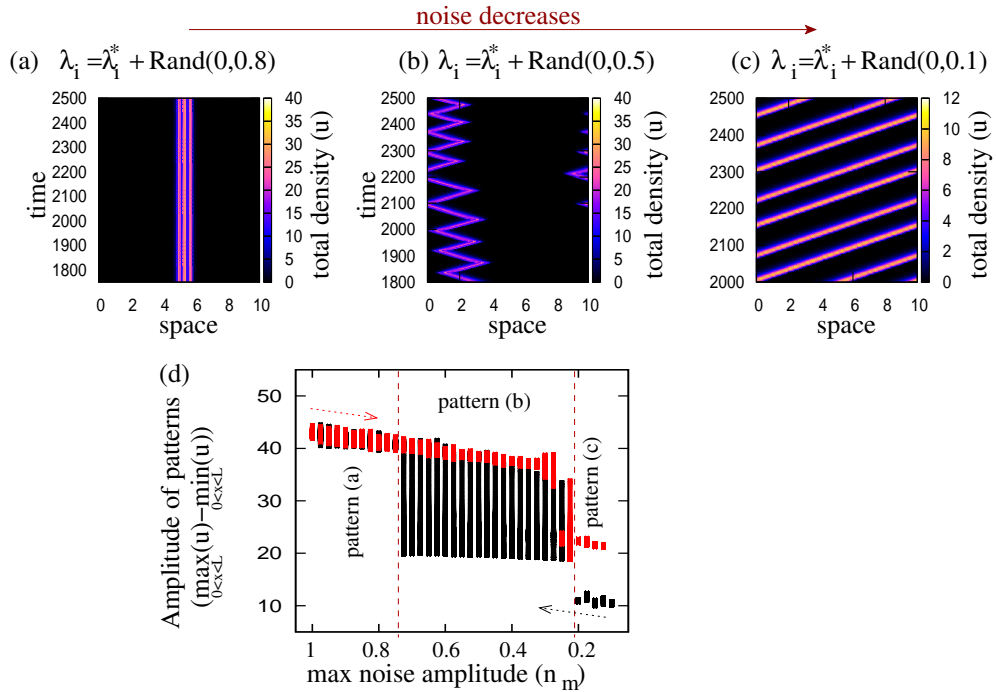


Fig. 9. Dynamics of model (1) when we vary the magnitude of the noise (n_m) that affects both random and directed turning: $\lambda_i = \lambda_i^* + \text{Rand}(0, n_m)$, $i = 1, 2$. (a) Stationary pulses for $n_m = 0.8$; (b) Chaotic zigzags for $n_m = 0.5$; (c) Travelling pulses for $n_m = 0.1$; (d) Bifurcation diagram for the amplitude of the total population density $u = u^+ + u^-$ corresponding to the different spatio-temporal patterns obtained as we vary the amplitude of the noise $n_m \in [0.1, 1]$. This local amplitude was calculated and graphed at every time step $t \in (1700, 2000)$. The dotted arrows show the direction in which the bifurcation diagram was obtained: $n_m = 1.0 \rightarrow n_m = 0.1$ (red branch) or $n_m = 0.1 \rightarrow n_m = 1.0$ (black branch). All other parameters are as in Table II.

since these bifurcation branches are unstable (with the corresponding patterns not persisting for time $t > 1000$), they are not shown in Figures 9(d) and 10(d).

Overall, the numerical simulations discussed in this Section suggest the co-existence of multiple (secondary) solution branches, with different amplitudes of $u = u^+ + u^-$, which can be reached by starting with different magnitudes of perturbations for parameter values. We emphasise that these bifurcation diagrams are not complete, being possible to discover also other branches with higher/lower amplitudes of solutions. A rigorous analytical investigation of the bifurcation structure can be performed, for example, via a weakly nonlinear analysis of the travelling pulse patterns obtained for $n_m \ll 1$ (or the stationary pulse patterns

obtained for $n_m < 1$), near the parameter value at which these patterns transform into zigzags (see Figures 9(d) and 10(d)). However, due to the complexity of such an investigation for the non-local hyperbolic models (1) (which involves perturbations of the spatially-heterogeneous travelling pulse; thus being more complex than the weakly nonlinear analysis of spatially-homogeneous states in [23]), this investigation is beyond the scope of the current study.

C. The effect of noise on both individual turning rates and perception of neighbours

Finally, we consider the combined effect of noise ($W(t) = \text{Rand}(0, n_m)$ with $n_m = 0.5$) on both the individual turning rates ($\lambda_{1,2}$) and on the perception of neighbours ahead/behind the reference individual ($p_{a,b}$). Figure 11 shows that

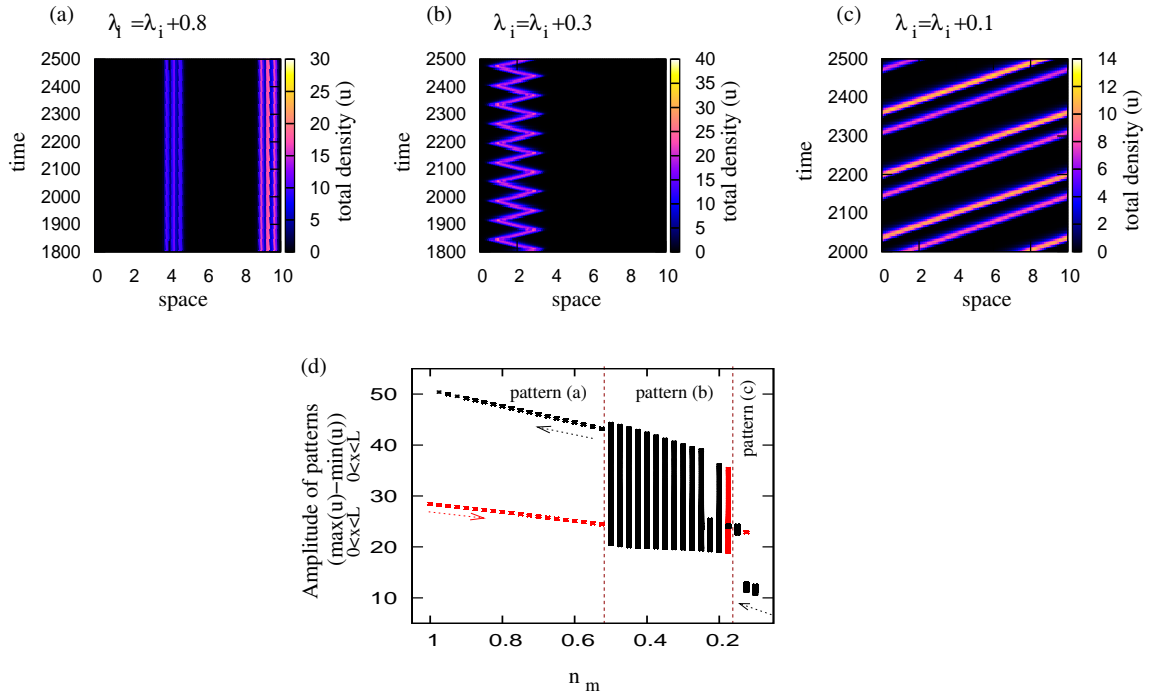


Fig. 10. Dynamics of deterministic model (1) when we vary $\lambda_{1,2}$ by a deterministic constant $n_m \in [0.1, 1]$ (while fixing $p_a = p_b = 1$): $\lambda_i = \lambda_i^* + n_m$. (a) Stationary pulses for $n_m = 0.8$; (b) Deterministic zigzags for $n_m = 0.5$; (c) Travelling pulses for $n_m = 0.2$; (d) Bifurcation diagram for the amplitude of the total population density $u = u^+ + u^-$, as calculated by graphing the local maximum amplitude of the pattern for every time step $t \in (1700, 2000)$. The dotted arrows show the direction in which the bifurcation diagram was obtained: $n_m = 1.0 \rightarrow n_m = 0.1$ (red branch) or $n_m = 0.1 \rightarrow n_m = 1.0$ (black branch). All other parameters are as in Table II.

while noise in the turning rates does seem to dominate the dynamics for $p_a \approx p_b$ (see the stationary chaotic zigzag in panel (a), and the travelling chaotic zigzag in panel (b)), increasing the perception strength of neighbours ahead (i.e., $p_a \gg p_b$) leads to a loss in the spatio-temporal patterns with the dynamics approaching a stable spatially homogeneous steady state, where $u^{*,+} \gg u^{*,-}$ (see the two lower figures in panel (c)).

Remark 4. We note that the linear stability analysis for the deterministic model (1) suggested that an increase in n_m for both $p_{a,b} = p_{a,b}^* + n_m$ and $\lambda_{1,2} = \lambda_{1,2}^* + n_m$ can lead to a stable steady state $(u^{*,+}, u^{*,-}) = (A^+, A^-)$ – see Figure 5(c). Given the observed numerical similarities between the bifurcation structure of the deterministic model (see Figure 9(d)) and the stochastic model (with $W(t) = \text{Rand}(0, n_m)$; see Figure 10(d)),

one could expect that in this particular case the stochastic stability results for the model with noise might also lead to stable states in a relatively similar parameter region, as the magnitude (n_m) of noise is increased. We need to emphasise that this is not a rigorous result (just an observation based on numerical simulations), as proving any extrapolation of mathematical results from the nonlocal deterministic model (1) to the nonlocal model with noise, is still an open problem. A linear stochastic stability analysis for this class of nonlocal hyperbolic models (with noise affecting turning behaviours) will be presented in a future study.

V. SUMMARY AND DISCUSSION

In this study, we considered a nonlocal hyperbolic model for the collective movement and self-organised behaviour of a population inhabiting a

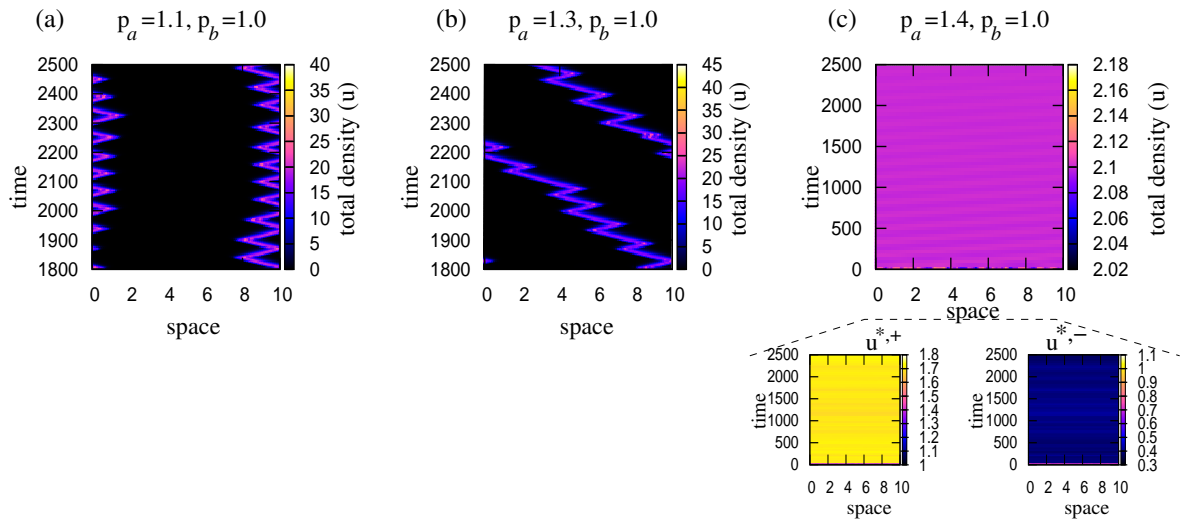


Fig. 11. Dynamics of system (1) when we increase p_a compared to p_b (to simulate a heterogeneous environment) and vary both $\lambda_{1,2}$ and $p_{a,b}$ by a stochastic term of maximum amplitude $n_m = 0.5$: $\lambda_{1,2} = \lambda_{1,2}^* + \text{Rand}(0, 0.5)$, $p_{a,b} = p_{a,b}^* + \text{Rand}(0, 0.5)$. (a) Stationary chaotic zigzags; (b) Travelling chaotic zigzags; (c) Spatially homogeneous state, with $u^{*,+} > u^{*,-}$.

1D domain (and thus formed of individuals moving left and right). Since noise in the environment can influence the interactions between individuals (e.g., how they perceive their neighbours, how they choose their movement direction, etc.) we also considered various stochastic terms.

We first focused on the deterministic version of the model and investigated the number and stability of the spatially-homogeneous steady states exhibited by this model. Then, we investigated numerically the stochastic model (with various stochastic terms, $W(t)$ and $W_1(t)$) and discussed the types of spatio-temporal patterns that can be exhibited by the model as we vary the amplitude of the noise (when we fix all other model parameters). We have shown that in the presence of noise, by increasing the difference between the perception of neighbours from ahead and behind (e.g., due to environmental heterogeneity), it is easy to lose the moving aggregation structure, and to obtain spatially heterogeneous solutions (where individuals are dispersed over the whole domain); see Figure 8. Moreover, the moving aggregation is more easily lost when we assume that the noise leads to an increase in the perception

of neighbours (by forcing individuals to modulate their communication to increase their chances of being detected [5]), compared to the case when we assume that noise can lead to either an increase or a decrease in the perception of neighbours.

We have also compared the spatio-temporal patterns obtained with the deterministic and stochastic versions of model (1); see Figures 9 and 10. The results showed that both models can exhibit similar patterns (at least for the parameter values considered in this study; see Table II): stationary pulses (i.e., aggregations), travelling pulses, zigzagging aggregations. However, the transition between these aggregations is slightly different between deterministic and stochastic cases (with the deterministic zigzagging pattern persisting in a smaller parameter region compared to the stochastic zigzagging pattern, and the presence of multiple branches of stationary pulses for the deterministic case compared to the stochastic case). The similarity between the patterns (and the transitions between them) observed with both the deterministic and stochastic models suggests that some of the stability results (for spatially homogeneous steady states) obtained with the deterministic model could

be extrapolated to the stochastic model.

We focused here only on a particular parameter space (as described in Table II), since the goal of our study was to investigate the effect of noise on one of the most common patterns exhibited by self-organised animal aggregations, namely travelling aggregations (i.e., travelling pulses). However, it is possible that noise can have different effects on different spatio-temporal patterns (see [22] for a summary of the patterns that can be exhibited by model (1)). Moreover, considering other types of communication mechanisms as in [22], [32] (e.g., unidirectional perception and emission of signals, or omnidirectional perception and emission of signals), could lead to different types of spatio-temporal patterns and different transitions between these patterns. All these aspects could be investigated in a future study.

Throughout this study, we focused on the numerical investigation of the noise and its effects on various patterns (and transitions between patterns). We note here that transitions between the deterministic patterns can be investigated analytically with the help of bifurcation theory (see, for example, [22], [39], [40], [41] for the application of the equivariant bifurcation theory to the classification and investigation of patterns exhibited by nonlocal hyperbolic models (1)). Given the complexity of the nonlocal models (1) the application of this theory (which involves perturbations of the spatial states $u^\pm(x, t)$) is not very straightforward. The bifurcation theory for stochastic systems is still in its infancy, and thus the analytical investigation of the transitions between the stochastic patterns shown in Figures 9 and 11 has never been attempted before (being currently an open problem).

Finally, we have shown numerically the existence of different types of (finite amplitude) spatio-temporal patterns exhibited by model (1): from stationary aggregations, to travelling pulses and chaotic and deterministic zigzags. Existence of mild and classical solutions for the nonlocal deterministic model (1) has been shown in [22], [29]. Future studies would need to focus on the existence of solutions for the stochastic model (1)

(including the existence of solutions with specific spatio-temporal structures mentioned above).

Acknowledgements: R.E acknowledges in kind support from the Fields Institute (Toronto, Canada), where part of this work has been carried on.

APPENDIX: SUMMARY OF MODEL PARAMETERS AND VARIABLES

In Table II we summarise the parameters that appear in model (1), and their values used for the numerical simulations. Since it is difficult to find biologically-realistic approximations for many of these parameter values (e.g., strengths of social interactions $q_{r,al,a}$, or perception intensities $p_{a,b}$), we choose to use values similar to those in [21], [22]. We acknowledge that while connecting these parameters to realistic biological situations (e.g., the behaviour of a particular animal species) would be the best approach, little available data on inter-individual interactions and quantifying animal communication makes it relatively difficult to take this approach. Finally, we need to emphasise that the aim of this study is not to focus on a particular animal species characterised by particular parameter values. Rather it is to investigate pattern formation and transitions between patterns as induced by external environmental and anthropogenic noise, in a class of mathematical models that could be applied to describe collective movement of animals, with the overall aim of generating new questions that could be investigated analytically.

REFERENCES

- [1] L. Rabin, B. McCowan, S. Hooper, D. Owings, Anthropogenic noise and its effect on animal communication: an interface between comparative psychology and conservation biology, *International journal of Comparative Psychology* 16 (2003) 172–192.
- [2] C. Kight, J. Swaddle, How and why environmental noise impacts animals: an integrative, mechanistic review, *Ecology Letters* 14 (2011) 1052–1061.
- [3] T. Ord, J. Stamps, Alert signals enhance animal communication, *Proc. Natl. Acad. Sci. USA* 105 (48) (2008) 18830–18835.

TABLE II

SUMMARY OF MODEL PARAMETERS AND THEIR VALUES USED FOR NUMERICAL SIMULATIONS. THESE PARAMETER VALUES ARE SIMILAR TO THOSE USED FOR SIMULATIONS IN [21], [22], [23].

Param.	Value	Description
γ	0.1	Constant individual speed
λ_1^*	0.1	Baseline value that approximates the constant random turning rate
λ_2^*	0.9	Baseline value that approximates the density-dependent turning rate
q_a	2	Strength of attractive inter-individual interactions
q_{al}	1	Strength of alignment/orientation inter-individual interactions
q_r	0.5	Strength of repulsive inter-individual interactions
p_a^*	1	Baseline perception strength of neighbours ahead (relative to the movement direction of the reference individual positioned at x)
p_b^*	1	Baseline perception strength of neighbours behind (relative to the movement direction of the reference individual positioned at x)
y_0	2	Constant parameter value that insures that for $u^\pm \approx 0$, the density-dependent component of the turning rate, $\lambda_2^* f[0, 0] \approx 0$ (and hence no turning in the absence of neighbours)
s_r	0.25	Spatial distance where the repulsion kernel has the strongest influence
s_{al}	0.5	Spatial distance where the alignment kernel has the strongest influence
s_a	1.0	Spatial distance where the attraction kernel has the strongest influence
m_r	$s_r/8$	Parameter that controls the width of the spatial ranges for the repulsive interactions
m_{al}	$s_{al}/8$	Parameter that controls the width of the spatial ranges for the alignment interactions
m_a	$s_a/8$	Parameter that controls the width of the spatial ranges for the attractive interactions
L	10	Domain size

- [4] F. VanDyke, R. Brocke, H. Shaw, B. Ackerman, T. Hemker, F. Lindzey, Reactions of mountain lions to logging and human activity, *J. Wildlife Management* 50 (1) (1986) 95–102.
- [5] M. Holt, D. Noren, V. Veirs, C. Emmons, S. Veirs, Speaking up: killer whales (*Orcinus orca*) increase their call amplitude in response to vessel noise, *Journal of the Acoustical Society of America* 125 (2009) EL27–EL32.
- [6] G. Rosenthal, D. Stuart-Fox, Environmental disturbances and animal communication, in: U. Candolin, B. Wong (Eds.), *Behavioral Response to a Changing World*, Oxford University Press, Oxford, 2012, Ch. 2, pp. 16–31.
- [7] H. Niwa, Self-organizing dynamic model of fish schooling, *J. Theor. Biol.* 171 (2) (1994) 123–136.
- [8] T. Vicsek, A. Czirók, E. Ben-Jacob, I. Cohen, O. Shochet, Novel type of phase transition in a system of self-driven particles, *Physical Review Letters* 75 (1995) 1226–1229.
- [9] G. Grégoire, H. Chaté, Onset of collective and cohesive motion, *Physical Review Letters* 92 (2004) 025702.
- [10] I. Couzin, J. Krause, R. James, G. Ruxton, N. Franks, Collective memory and spatial sorting in animal groups, *J. Theor. Biol.* 218 (2002) 1–11.
- [11] J. Gautrais, C. Jost, G. Theraulaz, Key behavioural factors in a self-organised fish school model, *Ann. Zool. Fennici* 45 (2008) 415–428.
- [12] U. Lopez, J. Gautrais, I. Couzin, G. Theraulaz, From behavioural analyses to models of collective motion in fish schools, *Interface Focus* 2 (2012) 693–707.
- [13] T. Vicsek, A. Zafeiris, Collective motion, *Physics Reports* 517 (3-4) (2012) 71–140.
- [14] M. Miguel, J. Parley, R. Pastor-Satorras, Effects of heterogeneous social interactions on flocking dynamics, *Physical Review Letters* 120 (2018) 068303.
- [15] J. Carrillo, M. Fornasier, G. Toscani, F. Vecil, Particle, kinetic, and hydrodynamic models of swarming, in: G. Naldi, L. Pareschi, G. Toscani (Eds.), *Mathematical Modelling of Collective Behaviour in Socio-Economic and Life Sciences*, Birkhäuser, Boston, 2010, pp. 297–336.
- [16] N. E. Saadi, A. Bah, Numerical simulations of a non-

- linear stochastic partial differential equation modeling phytoplankton aggregation, *J. Biological Systems* 23 (4) (2015) 1550032.
- [17] R. Carmona, R. Rozovskii (Eds.), *Stochastic partial differential equations: six perspectives*, American mathematical Society, Providence, Rhode Island, 1998.
- [18] J. Kim, On a stochastic scalar conservation law, *Indiana Univ. Math. J.* 52 (2003) 227–256.
- [19] J. Feng, D. Nualart, Stochastic scalar conservation laws, *J. Funct. Anal.* 255 (2008) 313–373.
- [20] G. Vallet, P. Wittbold, On a stochastic first-order hyperbolic equation in a bounded domain, *Infin. Dimens. Anal. Quantum Probab. Relat. Top.* 12 (2009) 613–651.
- [21] R. Eftimie, G. de Vries, M. A. Lewis, F. Lutscher, Modeling group formation and activity patterns in self-organizing collectives of individuals, *Bull. Math. Biol.* 69 (5) (2007) 1537–1566.
- [22] R. Eftimie, G. de Vries, M. A. Lewis, Complex spatial group patterns result from different animal communication mechanisms, *Proc. Natl. Acad. Sci.* 104 (17) (2007) 6974–6979.
- [23] R. Eftimie, G. de Vries, M. Lewis, Weakly nonlinear analysis of a hyperbolic model for animal group formation, *J. Math. Biol.* 59 (2009) 37–74.
- [24] R. Fetecau, Collective behaviour of biological aggregations in two dimensions: a nonlocal kinetic model, *Math. Models methods Appl. Sci.* 21 (2011) 1539–1569.
- [25] B. Pfister, A one-dimensional model for the swarming behaviour of *Myxobacteria*, in: W. Alt, G. Hoffmann (Eds.), *Lecture Notes on Biomath*, Vol. 89, Springer-Verlag, 1990, pp. 556–565.
- [26] F. Lutscher, Modeling alignment and movement of animals and cells, *Journal of Mathematical Biology* 45 (3) (2002) 234–260.
- [27] F. Lutscher, A. Stevens, Emerging patterns in a hyperbolic model for locally interacting cell systems, *J. Nonlinear Sci.* 12 (2002) 619–640.
- [28] L. Arlotti, A. Deutsch, M. Lachowicz, A discrete Boltzmann-type model of swarming, *Mathematical and Computer Modelling* 41 (2005) 1193–1201.
- [29] R. Fetecau, R. Eftimie, An investigation of a nonlocal hyperbolic model for self-organisation of biological groups, *J. Math. Biol.* 61 (4) (2010) 545–579.
- [30] J. Banasiak, M. Lachowicz, On a macroscopic limit of a kinetic model of alignment, *Mathematical Models and Methods in Applied Sciences* 23 (14) (2013) 2647–2670.
- [31] T. Platkowski, R. Illner, Discrete velocity models of the Boltzmann equation: a survey on the mathematical aspects of the theory, *SIAM Rev.* 30 (2) (1988) 213–255.
- [32] R. Eftimie, Hyperbolic and kinetic models for self-organized biological aggregations and movement: a brief review, *J. Math. Biol.* 65 (1) (2012) 35–75.
- [33] J. Kim, N. Mandrak, Assessing the potential movement of invasive fishes through the Welland Canal, *Journal of Great Lake Research* 42 (5) (2016) 1102–1108.
- [34] D. Golani, Impact of Red Sea fish migrants through the Suez Canal of the aquatic environment of the Eastern Mediterranean, *Bulletin of the Yale School for Forestry and Environment Studies* 103 (1998) 375–387.
- [35] Y. Katz, K. Tunström, C. Iannou, C. Huepe, I. Couzin, Inferring the structure and dynamics of interactions in schooling fish, *Proc. Natl. Acad. Sci. USA* 108 (46) (2011) 18720–18725.
- [36] D. Calovi, A. Litchinko, V. Lecheval, U. Lopez, A. P. Escudero, H. Chaté, C. Sire, G. Theraulaz, Disentangling and modeling interactions in fish with burst-and-coast swimming reveal distinct alignment and attraction behaviors, *PLoS Comput. Biol.* 14 (1) (2017) e1005933.
- [37] K. Hadeler, Reaction telegraph equations and random walk systems, in: S. van Strien, S. V. Lunel (Eds.), *Stochastic and spatial structures of dynamical systems*, Royal Academy of the Netherlands, North Holland, Amsterdam, 1996, pp. 133–162.
- [38] W. Press, S. Teukolsky, W. Vetterling, B. Flannery, *Numerical Recipes: The Art of Scientific Computing*, Cambridge University Press, 2007.
- [39] P.-L. Buono, R. Eftimie, Codimension-two bifurcations in animal aggregation models with symmetry, *SIAM J. Appl. Dyn. Syst.* 13 (4) (2014) 1542–1582.
- [40] P.-L. Buono, R. Eftimie, Analysis of Hopf/Hopf bifurcations in nonlocal hyperbolic models for self-organised aggregations, *Math. Models Methods Appl. Sci.* 24 (2) (2014) 327–357.
- [41] P.-L. Buono, R. Eftimie, Lyapunov-Schmidt and Centre Manifold reduction methods for nonlocal PDEs modelling animal aggregations, in: B. Toni (Ed.), *Mathematical Sciences with Multidisciplinary Applications*, Vol. 157, Springer, 2016, pp. 29–59.